

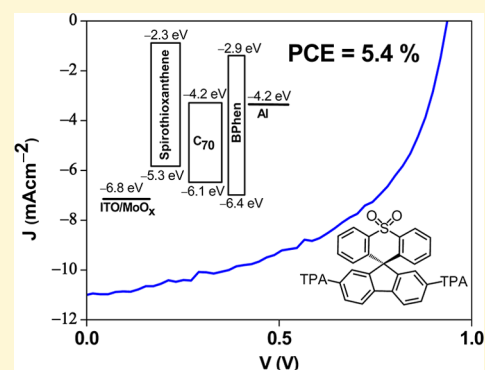
Hole-Transporting Spirothioxanthene Derivatives as Donor Materials for Efficient Small-Molecule-Based Organic Photovoltaic Devices

Chin-Yiu Chan,[†] Yi-Chun Wong,[†] Mei-Yee Chan,^{*,†} Sin-Hang Cheung,[‡] Shu-Kong So,[‡] and Vivian Wing-Wah Yam^{*,†}

[†]Department of Chemistry, The University of Hong Kong, Pokfulam Road, Hong Kong

[‡]Department of Physics, Hong Kong Baptist University, Kowloon Tong, Hong Kong

ABSTRACT: A new class of hole-transporting spirothioxanthene derivatives has been synthesized and characterized. Their photophysical, electrochemical and thermal properties have been studied. These compounds exhibit high hole mobilities of up to $1 \times 10^{-3} \text{ cm}^2 \text{ V}^{-1} \text{ s}^{-1}$, determined by using thin film transistor technique. In addition, these spirothioxanthene derivatives are promising donor materials in the construction of high performance organic photovoltaic (OPV) devices. With a very low dopant concentration of 7%, highly efficient small molecule-based OPV devices with high short-circuit current density of 10.83 mA cm^{-2} , open-circuit voltage of 0.94 V, and high power conversion efficiency of 5.40% (the highest PCE of 5.46%) have been realized.



INTRODUCTION

Organic photovoltaic (OPV) technology has aroused enormous attention in both academia and industry in recent years, owing to their distinct properties including great flexibility, higher transparency, lightweight, and lower manufacturing cost over the inorganic counterparts. Through a rational design on the molecular structure, a wide range of photoactive materials with interesting photophysical properties can be synthesized.^{1–7} Extensive studies on the development of novel photoactive materials and smart device architecture have boosted up the power conversion efficiencies (PCE) of OPV devices of up to 9.2% for a single cell and 10.6% for a tandem device.^{8,9} To date, the world-record OPV devices are made of conjugated polymer donors and solution-processed fullerene acceptors with a bulk heterojunction (BHJ) structure.

Although small molecule-based OPV devices are of equal importance as the polymer counterparts, the development of small molecule-based photoactive materials has received less attention owing to the relatively low PCE of such devices.^{10–14} In general, most of the small molecule-based donor materials have 1D or planar structures, and the mutually parallel orientation with fullerene acceptor would cause a serious charge recombination to quench the photogenerated excitons.^{15–19} More importantly, these donor materials, which are usually π -conjugated molecules, have excellent charge transfer character along the plane parallel to the π -conjugation, but considerably lower hole mobilities in the direction perpendicular to the molecular plane.^{15–19} This inevitably lowers the fill factor (FF) of the OPV devices. As reported by Tu and co-workers, the employment of 3D donor materials can significantly improve the photovoltaic responses.¹⁶ Particularly, the PCE of the devices (4.82%) is three times higher than that of devices based on 1D

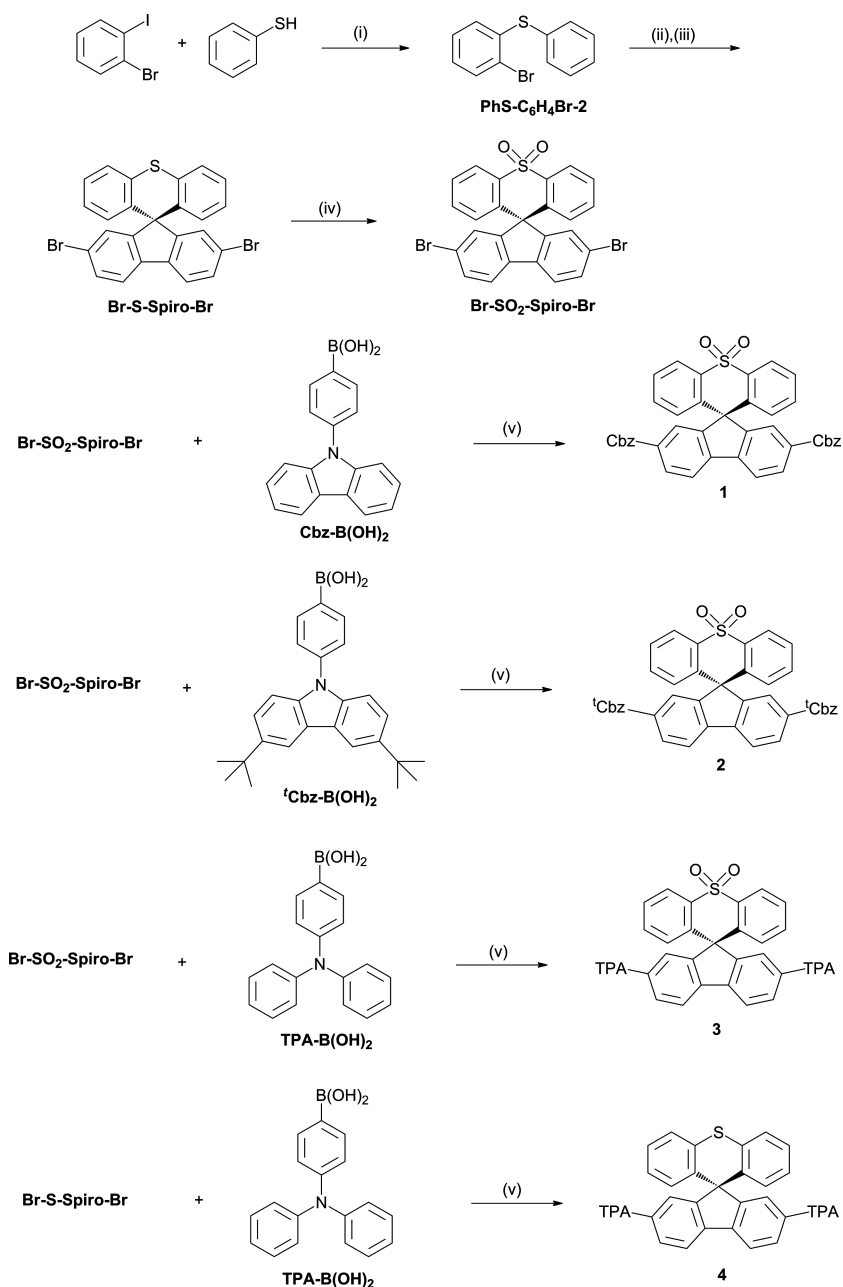
small molecules (1.69%).¹⁶ Such performance improvement is believed to be due to the suppression of intermolecular interactions by the steric bulky group in the 3D donor molecules.

From the design strategy, the donor materials must have a low bandgap with high absorption coefficient, in order to complement the absorption spectrum of the fullerene acceptor. On the other hand, Tang and co-workers recently demonstrated highly efficient OPV devices with PCE of up to 5.23% by employing a nonabsorbing 4,4'-cyclohexylidenebis[N,N-bis(4-methylphenyl)aniline] (TAPC) as donor in the BHJ.²⁰ This opens up new opportunities to make use of nonabsorbing organic materials as donor to realize highly efficient small molecule-based OPV devices.

Spirobifluorene and its derivatives are a benchmark class of p-type semiconductors in organic field-effect transistors and organic light-emitting devices (OLEDs) because of their excellent hole mobilities.^{21–23} Spirobifluorene has a 3D structure with a sp^3 carbon connecting two orthogonal π systems together. The rigid spiro-conjugation is found to enhance the hole-transporting property by hopping process.^{21–30} Taking its advantage of high luminescence quantum yield, spirobifluorene is also an ideal building block in the construction of stable blue light-emitting materials.^{24–27} The synthesis of metal-free organic dye sensitizers based on the use of the spiro group as π -conjugated spacers for dye-sensitized solar cells has been reported recently.^{28–30} The steric bulk of the spiro-configured central unit can effectively suppress aggregation-induced self-quenching as well as inhibit the intermolecular interactions,

Received: September 12, 2014

Revised: October 16, 2014

Scheme 1. Synthetic Scheme for 1–4^a

^a(i) CuI, *L*-Proline, K₂CO₃, DMF, 80 °C; (ii) ⁿBuLi, –78 °C, 2,7-dibromo-9-fluorenone; (iii) cat. triflic acid, CH₂Cl₂; (iv) *m*CPBA, DCM; (v) THF –aq. K₂CO₃ (2 M), [Pd(PPh₃)₄], reflux.

improving the photovoltaic properties.^{28–30} However, this class of materials has been rarely employed as photoactive materials in the fabrication of OPV devices, particularly because of their considerably low absorption coefficients within the visible spectrum. It was only until very recently that few examples of spirofluorene-based conjugated polymers or macromolecules as donor materials in OPV devices have been successfully reported, yielding highly efficient OPV devices with PCE of up to 4.6% and 4.82%, respectively.^{16,31} On the other hand, there are no literature reports on the use of small molecule-based heterocyclic spiro compounds as photoactive materials in the construction of high performance OPV devices.

Herein, we report the design and synthesis of a new class of heterocyclic spiro derivatives, namely spirothioxanthene, and the

successful demonstration for the first time of such compounds as promising candidates as donor materials in OPV devices. Noticeably, highly efficient small molecule-based OPV devices with PCE of up to 5.40% (the highest PCE of 5.46%) have been realized.

RESULTS AND DISCUSSION

Synthesis of Spirothioxanthene Derivatives. The synthetic route of compounds 1–4 is shown in Scheme 1. Conversion of tertiary alcohol intermediate to **Br-S-Spiro-Br** was carried out by ring closing reaction using catalytic amount of triflic acid. **Br-S-Spiro-Br** was then oxidized by 3-chloroperbenzoic acid to give compound **Br-SO₂-Spiro-Br**. Spirothioxanthene compounds 1–4 were synthesized using the

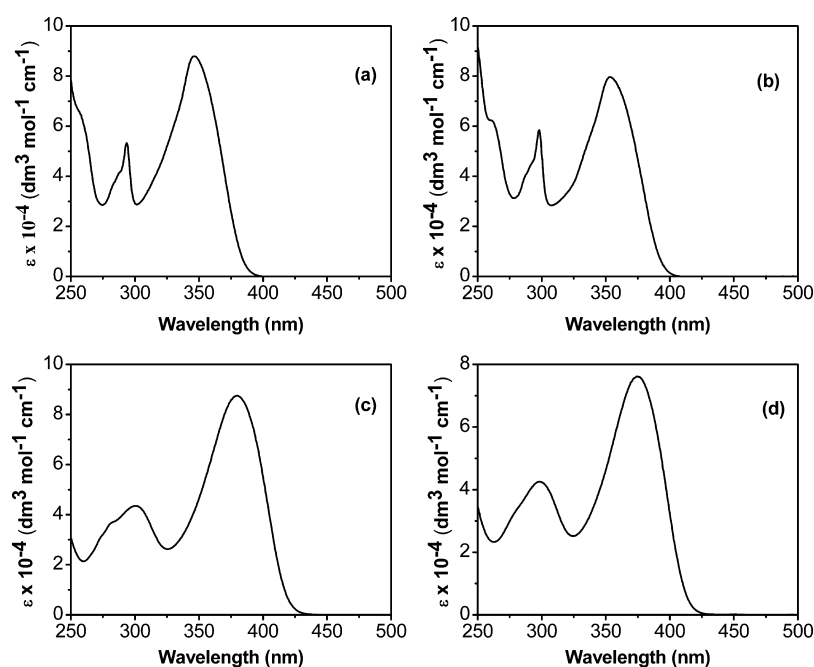


Figure 1. Electronic absorption spectrum of (a) 1, (b) 2, (c) 3, and (d) 4 in CH_2Cl_2 solution at 298 K.

standard Suzuki coupling reaction of **Br-S-Spiro-Br** or **Br-SO₂-Spiro-Br** with the corresponding boronic acid. All the reaction intermediates and compounds **1–4** have been characterized by ¹H NMR spectroscopy and HR-EI and FAB mass spectrometry. Satisfactory elemental analyses have also been obtained for compounds **1–4**.

Electronic Absorption Properties. The electronic absorption spectra of **1–4** were recorded in solutions of dichloromethane at 298 K. In general, the electronic absorption spectra of the spirothioxanthene compounds show similar absorption behavior. The absorption bands in the UV region could be assigned to the $\pi-\pi^*$ transitions with absorption maxima occurring at 346, 353, 380, and 375 nm for **1–4**, respectively, with extinction coefficients of up to $\sim 9 \times 10^4 \text{ dm}^3 \text{ mol}^{-1} \text{ cm}^{-1}$; while the absorption band at ca. 300 nm could be attributed to the $n-\pi^*$ transition of the triarylamine groups.¹⁷ In general, both the $\pi-\pi^*$ and $n-\pi^*$ transitions show a red shift in energy upon an increase in the electron richness of the electron-donating amine moiety on the spirothioxanthene derivatives, with carbazole being less electron-donating than di-*tert*-butylcarbazole than diphenylamine. This is consistent with the literature where stronger electron-donating group would destabilize both the π and the n orbitals more than the π^* orbital, giving rise to a reduction of the $\pi-\pi^*$ and $n-\pi^*$ energy gap and hence smaller transition energies [**1** (346 nm) > **2** (353 nm) > **3** (380 nm)].^{18,19} On the other hand, upon going from **3** to **4**, a blue shift in the $\pi-\pi^*$ transition energy is observed [**3** (380 nm) < **4** (375 nm)].^{18,19} This is in line with the lack of oxidation at the sulfur atom to sulfone in **4**, which results in the larger destabilization of the π^* orbital than the π orbital. Figure 1 shows the electronic absorption spectra of **1–4** and their electronic absorption spectral data are listed in Table 1.

Electrochemical Properties. The electrochemical behaviors of **1–4** have been investigated by cyclic voltammetry. The cyclic voltammograms were recorded in *N,N*-dimethylformamide in the presence of 0.1 M ⁿBu₄NPF₆. The spirothioxanthene compounds show one quasi-reversible to irreversible oxidation couple at +0.96 to +1.35 V versus standard calomel electrode

Table 1. Photophysical data of **1–4**

| Photophysical data for 1–4 | | |
|-----------------------------------|--------------------------|--|
| Compound | Medium | Absorption λ_{max} (nm) (ϵ_{max} ($\text{dm}^3 \text{ mol}^{-1} \text{ cm}^{-1}$)) |
| 1 | CH_2Cl_2 | 294 (54540), 346 (88140) |
| 2 | CH_2Cl_2 | 298 (58040), 353 (79470) |
| 3 | CH_2Cl_2 | 300 (43420), 380 (87320) |
| 4 | CH_2Cl_2 | 298 (42630), 375 (76390) |

(SCE), corresponding to the one-electron oxidation of the triarylamine unit (Figure 2). With the attachment of electron-rich triphenylamine groups, **3** and **4** display a quasi-reversible couple at +0.96 V vs SCE. On the other hand, the potential for oxidation is found to shift to more positive values when less electron-rich carbazole groups are attached. For instance, **1** displays an irreversible oxidation wave at +1.35 V whereas **2** shows a quasi-reversible oxidation couple at +1.20 V vs SCE. For reduction, all the compounds exhibit multiple reduction waves, in which the first reduction leads to a quasi-reversible reduction couple and the others give rise to irreversible waves. The reductions have been assigned as the sequential one-electron reduction of spirothioxanthene or the spirothioxanthene-dioxide core (Figure 3). The reduction waves are sensitive to the nature of electron-donating groups as well as the oxidation state of the sulfur atom. The electrochemical properties of **1–4** are summarized in Table 2, in which the highest occupied molecular orbital (HOMO) and the lowest unoccupied molecular orbital (LUMO) levels have been estimated from the potentials for oxidation and reduction, respectively.

Thermal Properties. The thermal properties of compounds **1–4** have been studied by thermogravimetric analysis (TGA). All the spirothioxanthene compounds show high thermal stability with decomposition temperatures (T_d) > 450 °C (i.e., T_d is defined as the temperature at which the material shows a 5% weight loss under a nitrogen atmosphere) (Figure 4). The thermal data of the spirothioxanthene compounds have been tabulated in Table 3.

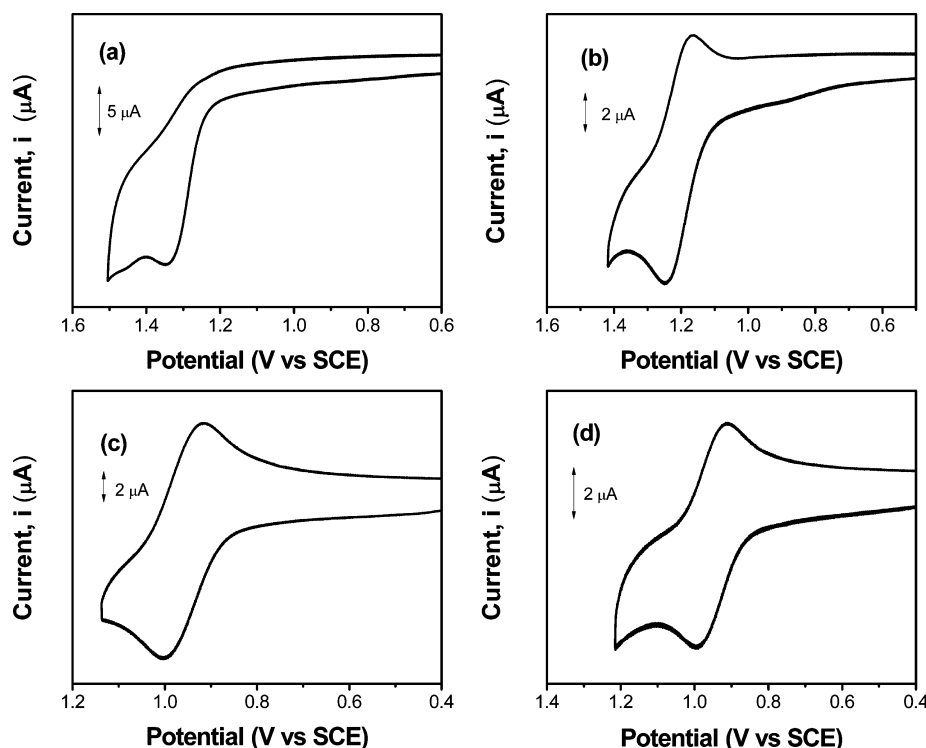


Figure 2. Cyclic voltammograms showing oxidative scans of (a) **1**, (b) **2**, (c) **3**, and (d) **4** in *N,N*-dimethylformamide (0.1 M $n\text{Bu}_4\text{NPF}_6$). Scan rate: 100 mV s^{-1} .

Photovoltaic Properties. To testify the applicability of the spirothioxanthene compounds as donor materials, we used BHJ OPV devices with the configuration of indium tin oxide (ITO)/molybdenum oxide (MoO_3) (2 nm)/ x % donor: C_{70} (60 nm)/bathophenanthroline (BPhen) (8 nm)/aluminum (Al) (100 nm) were fabricated, in which **1–4** as donor materials, whereas ITO, MoO_3 , C_{70} , BPhen and Al were used as the anode, anodic buffer layer, acceptor, exciton blocking layer, and cathode, respectively. For fair comparison, two control devices with the structures of ITO/ MoO_3 / C_{70} /BPhen/Al (i.e., C_{70} -only device) and ITO/ MoO_3 /7% TAPC: C_{70} /BPhen/Al (i.e., TAPC-doped device) were also prepared and tested under similar conditions. Under light illumination of 1 sun, the C_{70} -only device showed a poor performance with short-circuit current density (J_{SC}) of 1.25 mA cm^{-2} , an open-circuit voltage (V_{OC}) of 0.97 V, and a FF of 0.37. These correspond to a low PCE of 0.45%, consistent with other reports.^{20,37,38} The introduction of spirothioxanthene compounds as donor materials could dramatically improve the photovoltaic responses of OPV device. For instance, with increasing the doping concentration of **3** from 0 to 7%, the J_{SC} is found to increase from 1.25 to 10.83 mA cm^{-2} . Meanwhile, the FF is increased from 0.37 to 0.53. By keeping a high V_{OC} of 0.94 V, these correspond to a high PCE of 5.40% (the highest PCE of 5.46%), an order of magnitude higher than that of the C_{70} -only device (Figure 5). Further increase in the dopant concentration would cause a slight degradation of the photovoltaic responses. Similar performance improvement could be obtained by employing another spirothioxanthene compound as the donor (i.e., compound **4**). The optimized device (i.e., 7% compound **4**) illustrates a high J_{SC} of 10.81 mA cm^{-2} , a V_{OC} of 0.94 V, a FF of 0.49, and a PCE of 4.98% (the highest PCE of 5.02%). On the other hand, the photovoltaic responses of devices doped with carbazole-based spirothioxanthene (i.e., **1** and **2**) are relatively lower than those of devices with triphenylamine-based

compounds (i.e., **3** and **4**). The optimized devices doped with **1** and **2** give PCEs of 1.31 and 3.58%, respectively. The discrepancies in the device performance may be attributed to the blue-shifted absorption spectra and the lower-lying HOMO levels of **1** and **2**. To verify the accuracy of J_{SC} , we have examined the incident photon to current efficiencies (IPCEs) of the OPV devices, as depicted in Figure 6. For the C_{70} -only device, a rather low IPCE of 20.8% has been found at 380 nm. With the introduction of spirothioxanthene as donor, all the doped devices exhibit broad spectral responses in the range between 380 and 700 nm, roughly resembling the superposition of the absorption spectra of spirothioxanthene with peak maximum at 380 nm and C_{70} with peak maximum at 500 nm.²⁰ In addition, a pronounced improvement in the IPCE has been obtained. In particular, the IPCEs of the devices doped with **1–4** are found to be 30.5, 61.7, 79.0, and 73.7%, respectively, at 400 nm. These values are much higher than that of the C_{70} -only device (23.0%). It is worth noting that the J_{SC} values calculated from the integration of the IPCE spectra with the Air Mass (AM) 1.5 Global solar spectrum are in good agreement (i.e., within 10% uncertainty) with those measured from the current–voltage curves, which might be attributed to the degradation of the devices without encapsulation during measurements. Attempts had also been carried out to investigate the thermal annealing effects, in which the devices were annealed at 90 °C for 10 min. However, it was observed that the PCEs of all devices were dropped after thermal treatment, which might be attributed to a lower hole mobility in the spiro molecules arising from the change of the crystallinity. Table 4 lists the average cell parameters for the as-prepared devices doped with compounds **1–4**, in which the deviations were obtained from device-to-device variation of four identical devices.

Hole Mobility. As reported by Tang and co-workers, the hole mobility of donor materials plays a crucial role in determining the

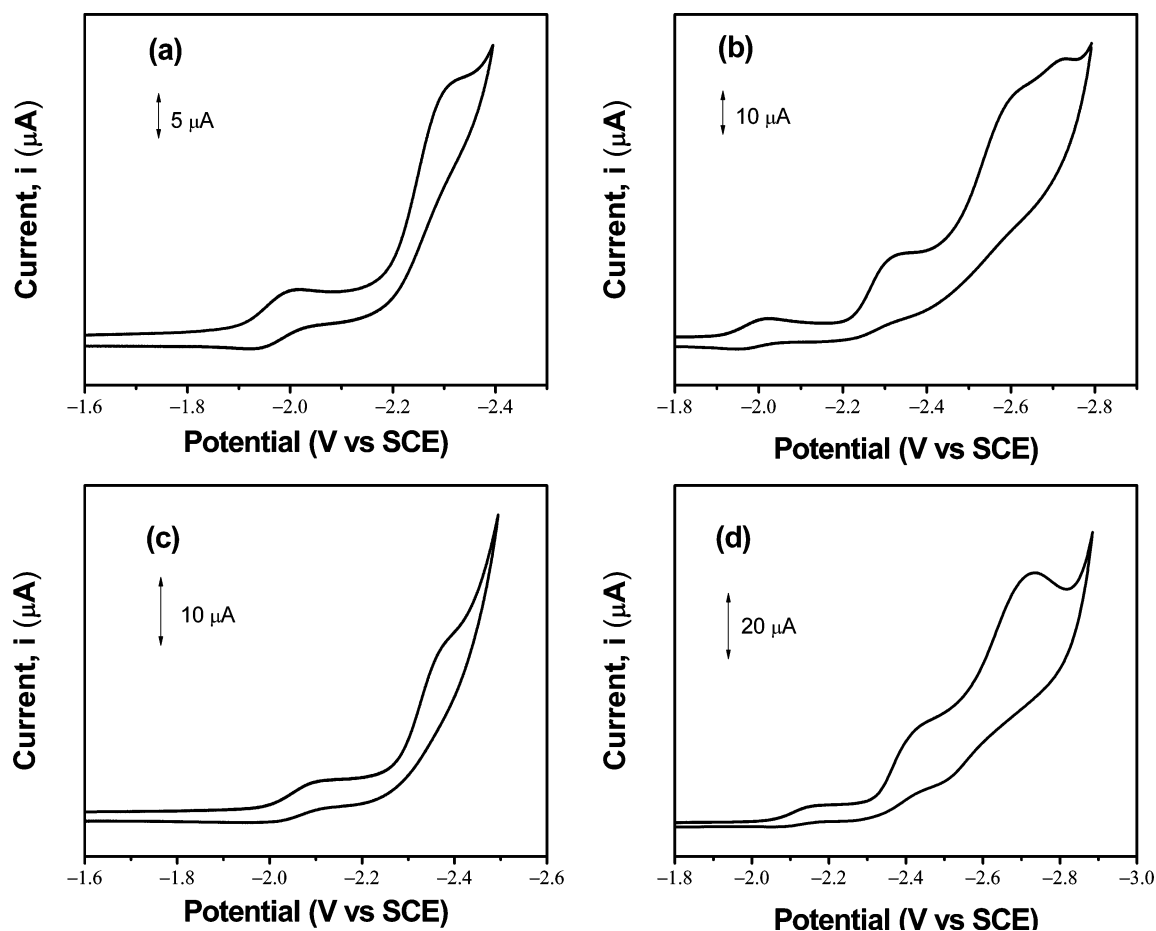


Figure 3. Cyclic voltammograms showing reductive scans of (a) **1**, (b) **2**, (c) **3**, and (d) **4** in *N,N*-dimethylformamide (0.1 M ⁿBu₄NPF₆). Scan rate: 100 mV s⁻¹.

Table 2. Electrochemical Properties of 1–4

| Compound | Oxidation $E_{1/2}$ (V ^b vs SCE) [E_{pa} (V ^b vs SCE)] (ΔE_p (mV)) | Reduction $E_{1/2}$ (V ^b vs SCE) [E_{pc} (V ^b vs SCE)] (ΔE_p (mV)) | HOMO (eV) ^e | LUMO (eV) ^f |
|----------|---|---|---------------------------|---------------------------|
| 1 | [+1.35] ^c | -1.97 (66), [-2.31] ^d | -5.70 | -2.38 |
| 2 | +1.20 (82) | -1.99 (63), [-2.32] ^d , [-2.61] ^d | -5.55 | -2.36 |
| 3 | +0.96 (86) | -2.05 (83), [-2.37] ^d | -5.31 | -2.30 |
| 4 | +0.96 (80) | -2.11 (82), [-2.42] ^d [-2.73] ^d | -5.31 | -2.24 |

^a0.1 M ⁿBu₄NPF₆ (TBAH) as supporting electrolyte at room temperature; scan rate 100 mV s⁻¹. ^b $E_{1/2} = (E_{pa} + E_{pc})/2$; E_{pa} and E_{pc} are peak anodic and peak cathodic potentials, respectively. ^cIrreversible oxidation wave. The potential refers to E_{pa} , which is the anodic peak potential. ^dIrreversible reduction wave. The potential refers to E_{pc} , which is the cathodic peak potential. ^e $E_{HOMO} = -(E_{ox} + 4.35)$ eV. ^f $E_{LUMO} = -(E_{red} + 4.35)$ eV.

performance of the OPV devices.²⁰ To correlate with the photovoltaic properties, we determined hole mobilities of the spirothioxanthene compounds in a thin film transistor (TFT) configuration at room temperature.³⁹ Specifically, compounds **3** and **4** which exhibit a good photovoltaic performance have been examined. The hole mobility of TAPC was also studied for a fair comparison. Figure 7 shows the output and transfer characteristics of the fabricated OTFTs. At a large gate voltage (V_G) of -50 V, TAPC exhibits a larger source-to-drain current (I_{DS}) between 2.5 and 3.0 μ A, whereas both spirothioxanthene compounds **3** and **4** show smaller I_{DS} . TAPC also exhibits higher mobilities of 2.5×10^{-3} and 3.1×10^{-3} cm² V⁻¹ s⁻¹ in the linear and saturation regions, respectively. With the attachment of the more electron-rich triphenylamine groups, compound **4** demonstrates comparable hole mobilities, where the linear mobilities (μ_{Linear}) and saturation mobilities (μ_{Sat}) are found to be

1.4×10^{-3} and 8.5×10^{-4} cm² V⁻¹ s⁻¹, respectively. On the other hand, with oxidation of the sulfur atom, compound **3** shows smaller hole mobilities (i.e., $\mu_{Linear} = 2.0 \times 10^{-4}$ cm² V⁻¹ s⁻¹; $\mu_{Sat} = 1.4 \times 10^{-4}$ cm² V⁻¹ s⁻¹). In correlating with the photovoltaic responses, it seems that hole mobilities measured by the OFET method are not the determining factors governing the device performance. Although TAPC possesses a higher hole mobility than the spirothioxanthene compounds, the PCEs of devices doped with compounds **3** and **4** are found to be higher than that of TAPC (4.38%), as shown in Table 4. The higher PCEs are likely to be due to the higher V_{OC} values for devices doped with **3** and **4**, which may be ascribed to a reduced dark current. As depicted in Figure 8, the devices doped with **3** and **4** exhibit a reduced dark current at -1 V than that of a similar device doped with TAPC. The reduced dark current can significantly reduce the electron leakage current and results in an increase in the V_{OC}

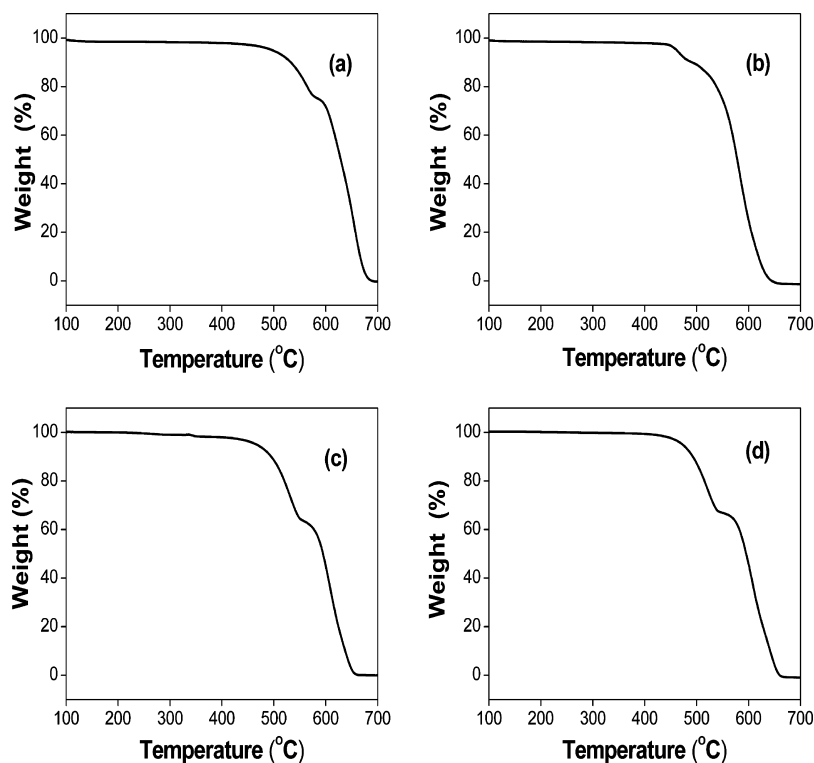


Figure 4. TGA thermograms of (a) 1, (b) 2, (c) 3, and (d) 4. Heating rate: $10\text{ }^{\circ}\text{C min}^{-1}$ under a nitrogen atmosphere.

Table 3. Thermal Properties for 1–4

| Compound | T_{decomp} ($^{\circ}\text{C}$) ^a |
|----------|---|
| 1 | 497 |
| 2 | 462 |
| 3 | 466 |
| 4 | 473 |

^aDetermined by thermogravimetric analysis. Heating rate: $10\text{ }^{\circ}\text{C min}^{-1}$ under a nitrogen atmosphere. T_{decomp} was determined at 5% weight loss.

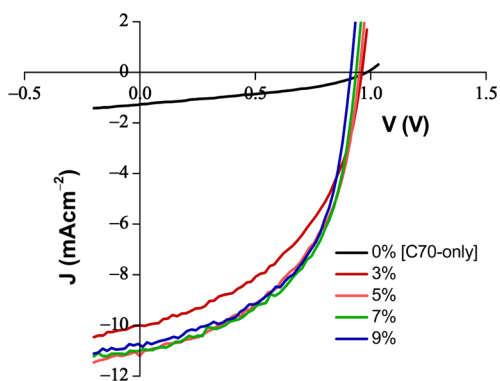


Figure 5. J - V characteristics of devices doped with 3 at different concentrations under light illumination of 1 sun.

of the OPV devices.⁴⁰ Nevertheless, the findings clearly demonstrate for the first time that spirothioxanthene compounds are a promising class of donor materials that warrants further exploration to realize high-performance small-molecule-based OPV devices.

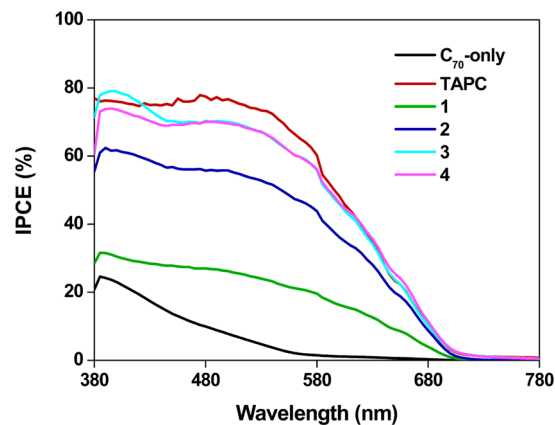


Figure 6. IPCE of devices doped with 7% donor material.

CONCLUSION

In summary, a new class of spirothioxanthene compounds has been successfully designed and synthesized. The functionalization of the spiro core with various triarylamine groups and the modification of the heteroatom of the spiro core have been shown to be capable of tuning both the photophysical and electrochemical properties of the spirothioxanthene compounds. These compounds exhibit high hole mobilities of up to $1 \times 10^{-3}\text{ cm}^2\text{ V}^{-1}\text{ s}^{-1}$, comparable to the prototypical hole-transporting TAPC. More importantly, spirothioxanthene compounds are promising donor materials for the construction of high performance OPV devices. With a very low dopant concentration of 7%, highly efficient small-molecule-based OPV devices with PCE of up to 5.40% (the highest PCE of 5.46%) have been realized.

Table 4. Key Photovoltaic Responses for the As-Prepared Devices without and with Donor Material

| Compound | Dopant Conc. (%) | J_{sc} Calcd (mA cm^{-2}) | J_{sc} (mA cm^{-2}) | V_{oc} (V) | FF | PCE (%) |
|-----------------------|------------------|--|----------------------------------|--------------|-------------|-------------|
| C ₇₀ -Only | 0 | 1.15 | 1.25 ± 0.03 | 0.97 ± 0.02 | 0.37 ± 0.01 | 0.45 ± 0.02 |
| TAPC | 7 | 10.62 | 10.73 ± 0.47 | 0.85 ± 0.01 | 0.48 ± 0.01 | 4.38 ± 0.13 |
| 1 | 3 | 2.86 | 2.90 ± 0.12 | 1.06 ± 0.01 | 0.27 ± 0.01 | 0.83 ± 0.04 |
| | 5 | 3.12 | 3.04 ± 0.11 | 1.10 ± 0.01 | 0.26 ± 0.01 | 0.87 ± 0.03 |
| | 7 | 3.70 | 3.86 ± 0.17 | 1.08 ± 0.01 | 0.27 ± 0.01 | 1.13 ± 0.05 |
| | 9 | 4.27 | 4.17 ± 0.09 | 1.08 ± 0.01 | 0.29 ± 0.01 | 1.31 ± 0.04 |
| | 3 | 6.44 | 6.62 ± 0.04 | 1.16 ± 0.01 | 0.34 ± 0.01 | 2.61 ± 0.09 |
| 2 | 5 | 7.42 | 7.67 ± 0.08 | 1.17 ± 0.01 | 0.35 ± 0.01 | 3.14 ± 0.03 |
| | 7 | 7.94 | 8.57 ± 0.12 | 1.16 ± 0.01 | 0.36 ± 0.01 | 3.58 ± 0.02 |
| | 9 | 8.15 | 8.35 ± 0.02 | 1.16 ± 0.01 | 0.37 ± 0.01 | 3.58 ± 0.01 |
| 3 | 3 | 9.78 | 9.78 ± 0.22 | 0.96 ± 0.01 | 0.47 ± 0.01 | 4.41 ± 0.10 |
| | 5 | 9.77 | 10.86 ± 0.16 | 0.95 ± 0.01 | 0.50 ± 0.01 | 5.16 ± 0.03 |
| | 7 | 10.00 | 10.83 ± 0.14 | 0.94 ± 0.01 | 0.53 ± 0.01 | 5.40 ± 0.06 |
| | 9 | 9.84 | 10.60 ± 0.11 | 0.92 ± 0.01 | 0.54 ± 0.01 | 5.27 ± 0.07 |
| 4 | 3 | 9.81 | 10.14 ± 0.17 | 0.96 ± 0.01 | 0.43 ± 0.01 | 4.19 ± 0.09 |
| | 5 | 10.03 | 10.94 ± 0.41 | 0.95 ± 0.01 | 0.48 ± 0.01 | 4.99 ± 0.08 |
| | 7 | 9.99 | 10.81 ± 0.11 | 0.94 ± 0.01 | 0.49 ± 0.01 | 4.98 ± 0.05 |
| | 9 | 9.97 | 10.67 ± 0.05 | 0.93 ± 0.01 | 0.49 ± 0.01 | 4.86 ± 0.09 |

EXPERIMENTAL SECTION

Materials. All chemicals used for synthesis were of analytical grade and were purchased from Sigma–Aldrich Chemical Co. 4-(Diphenylamino)phenylboronic acid, 4-(9*H*-carbazol-9-yl)phenylboronic acid, 2,7-dibromo-9-fluorenone, 4-(3,6-di-*tert*-butyl-9*H*-carbazol-9-yl)phenylboronic acid and (2-bromophenyl)(phenyl)sulfane (PhS–C₆H₄Br–2) were synthesized according to the literature reported procedures.^{32–36}

Physical Measurements and Instrumentation. ¹H NMR spectra were recorded using a Bruker DPX-300 (300 MHz) or a Bruker Avance 400 (400 MHz) Fourier-transform NMR spectrometer with chemical shifts reported relative to tetramethylsilane, (CH₃)₄Si. Positive-ion EI and FAB mass spectra were recorded using a Thermo Scientific DFS high-resolution magnetic sector mass spectrometer. The electronic absorption spectra were obtained using a Hewlett–Packard 8452A diode array spectrophotometer. Cyclic voltammetric measurements were performed by using a CH Instruments, Inc. model CHI 620A electrochemical analyzer. Electrochemical measurements were performed in dichloromethane solutions with 0.1 mol dm^{−3} nBu₄NPF₆ as supporting electrolyte at room temperature. The reference electrode was a Ag/AgNO₃ (0.1 mol dm^{−3} in acetonitrile) electrode, and the working electrode was a glassy carbon electrode (CH Instruments, Inc.) with a platinum wire as the counter electrode. The working electrode surface was first polished with 1 μm alumina slurry (Linde) on a microcloth (Buehler Co.) and then with 0.3 μm alumina slurry. It was then rinsed with ultrapure deionized water and sonicated in a beaker that contained ultrapure water for 5 min. The polishing and sonicating steps were repeated twice, and then the working electrode was finally rinsed under a stream of ultrapure deionized water. The ferrocenium/ferrocene couple (Fc⁺/Fc) was used as the internal reference. All solutions for electrochemical studies were deaerated with prepurified argon gas prior to measurements. Thermal Gravimetric Analysis was performed by thermal gravimetric analyzer (PerkinElmer TGA 7) with a heating rate of 10 °C min^{−1} under a nitrogen atmosphere.

Synthesis and Characterization. *Br–S–Spiro–Br.* (2-Bromophenyl)(phenyl)sulfane (265 mg, 1 mmol) was dissolved in dry THF and degassed for 15 min. The resulting mixture was cooled to −78 °C under nitrogen, and ⁿBuLi (1.6 M in hexanes, 0.7 mL, 1.1 mmol) was added in a dropwise manner. The resulting mixture was stirred at −78 °C for 1 h, and then 2,7-dibromo-9-fluorenone (328 mg, 1 mmol) was added in one portion. The reaction mixture was kept at −78 °C for another hour before warming to room temperature, and then stirred overnight. The resulting mixture was quenched with deionized water and extracted with dichloromethane for three times. The combined organic layer was then washed with deionized water. The solution was

dried over anhydrous MgSO₄ and filtered. The solvent was evaporated to dryness under vacuum. The crude solid was washed with hexane, filtered and used without further purification. The tertiary alcohol intermediate was dissolved in dichloromethane solution. A few drops of triflic acid were added. The reaction was monitored by TLC analysis until no starting material could be detected. The reaction was washed with deionized water and the organic layer was dried over anhydrous MgSO₄. The organic layer was filtered and evaporated to dryness under vacuum. The crude product was purified by column chromatography using hexane as eluent. Further purification was achieved by recrystallization of the product from dichloromethane-methanol. Yield: 379 mg (75%) ¹H NMR (300 MHz, CDCl₃, 298 K, relative to Me₄Si): δ 6.49 (d, 2H, 8.0 Hz), 6.92 (t, 2H, 8.0 Hz), 7.19 (t, 2H, 8.0 Hz), 7.42 (d, 2H, 8.0 Hz), 7.51 (d, 2H, 8.0 Hz), 7.61 (d, 2H, 8.0 Hz), 7.67 (s, 2H). HRMS (Positive EI) calcd for C₂₅H₁₄Br₂S: *m/z* = 505.9334; found: 505.9166 [M]⁺.

Br–SO₂–Spiro–Br. Br–S–Spiro–Br (506 mg, 1 mmol) was dissolved in dichloromethane and was cooled to 0 °C. *m*CPBA (90 mg) was added and the resulting mixture was slowly warmed to room temperature, and stirred overnight. The reaction was quenched with aqueous Na₂S₂O₅ (2 M) and then washed with aqueous Na₂CO₃ (2 M), deionized water. The organic layer was dried over anhydrous MgSO₄. The organic layer was filtered and evaporated to dryness under vacuum. The crude product was purified by column chromatography using dichloromethane-hexane as eluent. Further purification was achieved by recrystallization of the product from dichloromethane-methanol. Yield: 484 mg (90%) ¹H NMR (300 MHz, CDCl₃, 298 K, relative to Me₄Si): δ 6.57 (d, 2H, 8.0 Hz), 7.32 (t, 2H, 8.0 Hz), 7.46 (s, 2H), 7.51 (d, 2H, 8.0 Hz), 7.58 (d, 2H, 8.0 Hz), 7.68 (d, 2H, 8.0 Hz), 8.26 (d, 2H, 8.0 Hz). MS (Positive FAB) calcd for C₂₅H₁₄O₂Br₂S: *m/z* = 538.3; found: 538.7 [M]⁺.

General Procedure for Compounds 1–4. Compounds 1–4 were synthesized according to the standard Suzuki coupling reaction. The precursor, *Br–S–Spiro–Br* or *Br–SO₂–Spiro–Br* (1 mmol), was dissolved in a mixture of aqueous K₂CO₃ (2 M) solution (4 mL) and THF (80 mL). After that, the corresponding boronic acid (3 mmol) was added to the reaction mixture. The solvent was degassed for 15 min and [Pd(PPh₃)₄] catalyst (0.1 mmol) was added. The reaction mixture was heated to reflux overnight. The crude reaction mixture was extracted with dichloromethane for at least three times. Then, the organic layer was washed with deionized water several times. The organic layer was dried over anhydrous MgSO₄ and filtered. The solvent was evaporated to dryness under vacuum. The crude product was purified by column chromatography using dichloromethane-hexane as eluent. Further purification was achieved by recrystallization of the product with THF-pentane or chloroform-acetone.

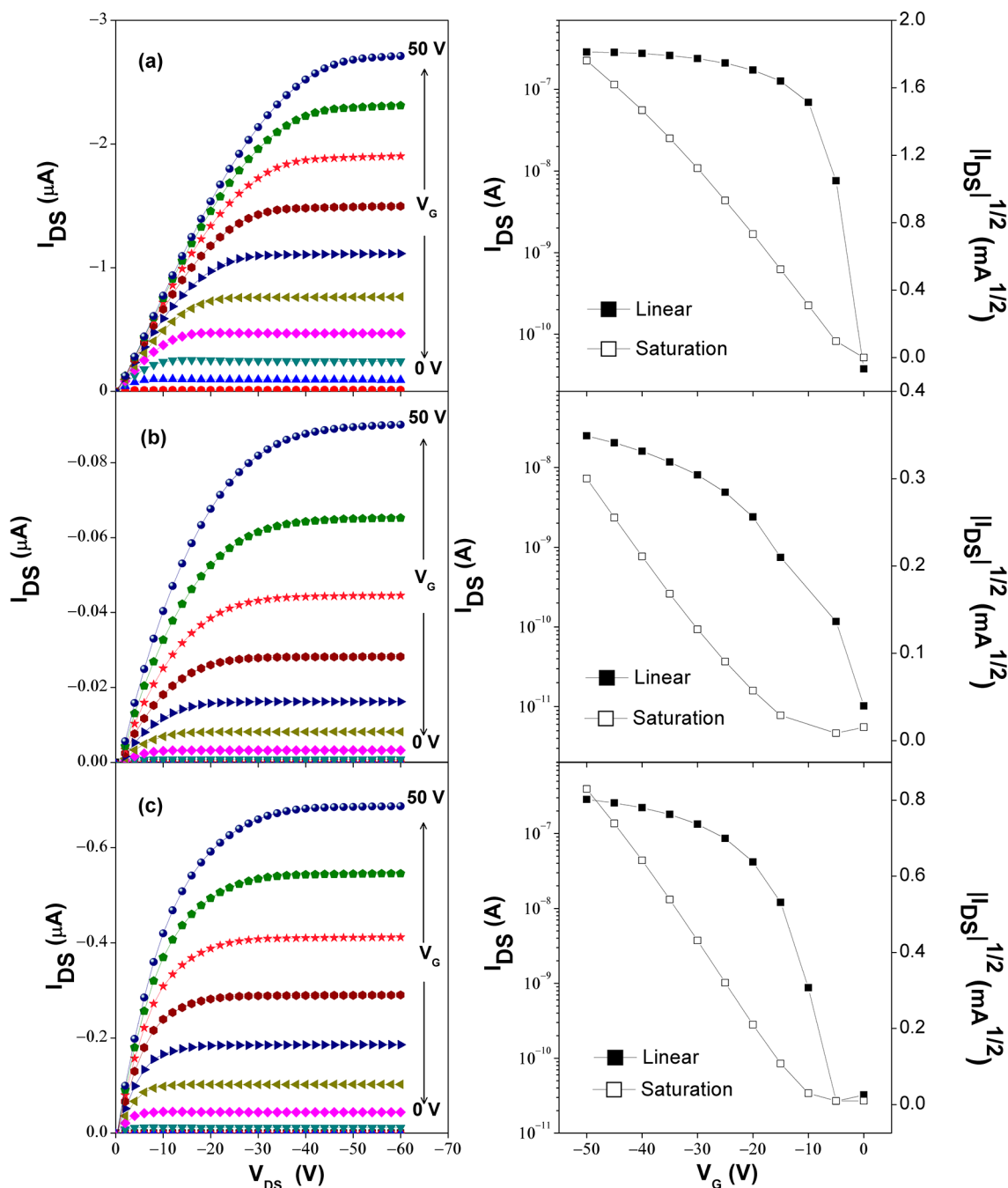


Figure 7. Output and transfer characteristics of the fabricated OTFTs based on (a) TAPC, (b) 3, and (c) 4.

Cbz-SO₂-Spiro-Cbz (1). Yield: 690 mg (80%). ¹H NMR (400 MHz, CDCl₃, 298 K, relative to Me₄Si): δ 6.80 (d, 2H, 8.0 Hz), 7.27–7.30 (m, 4H), 7.37–7.43 (m, 10H), 7.52–7.59 (m, 6H), 7.75–7.79 (m, 6H), 7.84 (d, 2H, 8.0 Hz), 8.02 (d, 2H, 8.0 Hz), 8.13 (d, 4H, 8.0 Hz), 8.32 (d, 2H, 8.0 Hz). MS (Positive FAB) calcd for C₆₁H₃₈O₂N₂S: m/z = 863.0; found: 863.3 [M]⁺. Elemental anal. Calcd (%) for C₆₁H₃₈O₂N₂S·0.5(CH₃)₂O: C 84.04, H 4.66, N 3.16. Found: C 84.33, H 4.50, N 3.13.

^tCbz-SO₂-Spiro-^tCbz (2). Yield: 814 mg (75%). ¹H NMR (400 MHz, CDCl₃, 298 K, relative to Me₄Si): δ 1.46 (s, 36H), 6.79 (d, 2H, 8.0 Hz), 7.37–7.43 (m, 10H), 7.52–7.59 (m, 6H), 7.75–7.79 (m, 6H), 7.84 (d, 2H, 8.0 Hz), 8.01 (d, 2H, 8.0 Hz), 8.12 (s, 4H), 8.31 (d, 2H, 8.0 Hz). MS (Positive FAB) calcd for C₇₇H₇₀O₂N₂S: m/z = 1087.5; found: 1086.1 [M–1]⁺. Elemental anal. Calcd (%) for C₇₇H₇₀O₂N₂S: C 85.04, H 6.49, N 2.58. Found: C 84.84, H 6.74, N 2.41.

TPA-SO₂-Spiro-TPA (3). Yield: 560 mg (68%). ¹H NMR (400 MHz, CDCl₃, 298 K, relative to Me₄Si): δ 6.71 (d, 2H, 8.0 Hz), 6.99–

7.08 (m, 16H), 7.23 (t, 8H, 7.5 Hz), 7.28 (d, 2H, 8.0 Hz), 7.37 (d, 4H, 8.0 Hz), 7.46 (t, 2H, 8.0 Hz), 7.60 (s, 2H), 7.67 (d, 2H, 8.0 Hz), 7.87 (d, 2H, 8.0 Hz), 8.24 (d, 2H, 8.0 Hz). MS (Positive FAB) calcd for C₆₁H₄₂O₂N₂S: m/z = 867.1; found: 867.3 [M]⁺. Elemental anal. Calcd (%) for C₆₁H₄₂O₂N₂S·0.5C₃H₁₂: C 84.45, H 5.36, N 3.10. Found: C 84.17, H 5.08, N 3.15.

TPA-S-Spiro-TPA (4). Yield: 584 mg (70%). ¹H NMR (400 MHz, CD₂Cl₂, 298 K, relative to Me₄Si): δ 6.63 (d, 2H, 8.0 Hz), 6.89 (t, 2H, 8.0 Hz), 6.99–7.06 (m, 16H), 7.15 (t, 2H, 8.0 Hz), 7.23 (t, 8H, 7.4 Hz), 7.40–7.43 (m, 6H), 7.64 (d, 2H, 8.0 Hz), 7.78 (s, 2H), 7.84 (d, 2H, 8.0 Hz). HRMS (Positive EI) calcd for C₆₁H₄₂SN₂: m/z = 834.3063; found: 834.2063 [M]⁺. Elemental anal. Calcd (%) for C₆₁H₄₂SN₂·(CH₂)₄O: C 86.06, H 5.56, N 3.09. Found: C 86.05, H 5.42, N 3.30.

OPV Device Fabrication and Characterization. OPV devices were grown on indium tin oxide (ITO)-coated glass substrates with sheet resistance of 25 ohm square⁻¹. The substrates were cleaned with

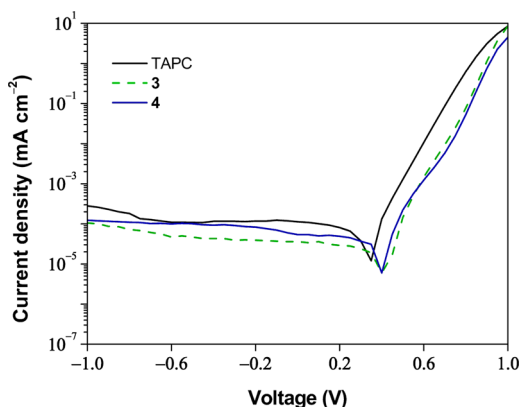


Figure 8. Dark current of the OPV devices doped with TAPC, 3, and 4.

Decon 90, rinsed with deionized water then dried in an oven, and finally treated in an ultraviolet-ozone chamber. A 2 nm anodic buffer layer of MoO_3 , a 60 nm blend of active layer containing spirothioxanthene donor and C_{70} acceptor, a 8 nm exciton blocking layer of BPhen, and a 100 nm top cathode of aluminum, were sequentially thermally evaporated onto the substrates in vacuum chamber. All organic and metal layers were successively deposited at a rate of $0.1\text{--}0.2\text{ nm s}^{-1}$ in a Trovato Mfg. Inc. high vacuum evaporator under a base pressure of $<5 \times 10^{-6}$ Torr without vacuum break. Film thicknesses were determined in situ by calibrated oscillating quartz-crystal sensors. Shadow masks were used to define the patterns of organic and cathode layers to make four 0.1 cm^2 identical devices on each substrate. Current–voltage characteristics of the solar cells were measured using a programmable Keithley model 2400 power source. The photocurrent was measured under illumination from an Oriel 300 W solar simulator equipped with AM 1.5 G (AM: air mass; G: global) filter, and the light intensity was measured using an Oriel silicon reference cell equipped with KG-5 filter. For the external quantum efficiency measurements, devices were irradiated with monochromatic light of variable wavelength by using an Oriel Quantum Efficiency/IPCE Measurement Kit equipped with Oriel Cornerstone 260 1/4 m monochromator with a 300 W xenon arc lamp. The intensity of the source at each wavelength was determined using a calibrated silicon detector. The photocurrent under short-circuit conditions was recorded by using a dual channel radiometer at 10 nm intervals for each device. All experiments and measurements were carried out at room temperature under ambient environment without device encapsulation.

OTFT Device Fabrication and Characterization. OTFT devices were fabricated on heavily p-doped silicon substrates that had been thermally grown with 300 nm of silicon dioxide (SiO_2) as the dielectric layer. Before fabrication, the substrates were first cleaned by filtered acetone, followed by UV-ozone treatment. After treatment, a 30 nm thick polystyrene (PS) dielectric layer was spin-coated onto the SiO_2 layer at 2000 rpm from 0.45 wt % 1,1,2-trichloroethane solution. The samples were then baked inside a vacuum oven overnight at 60°C and were transferred into a vacuum chamber. An active layer was formed by evaporating spirothioxanthene onto the PS layer. The source and drain electrodes composed of a 20 nm thick MoO_3 layer and a 100 nm Au layer were prepared by thermal evaporation at a base pressure of 1×10^{-6} Torr. The presence of the MoO_3 interlayer was used as surface modification layer to facilitate hole injection into the active layer. The channel width (W) and length (L) were 6 mm and $50\ \mu\text{m}$. After fabrication, the samples were transferred immediately to a temperature controlled cryostat for electrical measurements. All TFT measurements were performed in vacuum. The TFT mobilities in the linear (μ_{linear}) and saturation (μ_{sat}) regions were evaluated by standard equations, i.e., $I_{\text{DS}} = (W/L)\mu_{\text{linear}}C_i(V_G - V_T)V_{\text{DS}}$ and $I_{\text{DS}} = (W/2L)\mu_{\text{sat}}C_i(V_G - V_T)^2$, where I_{DS} is the measured source-to-drain current, C_i is the capacitance of the gate dielectric per unit area; V_{DS} , V_G , and V_T are the applied source to drain voltage, the gate voltage, and the threshold voltage of the OTFT, respectively.

AUTHOR INFORMATION

Corresponding Authors

*E-mail: wwyam@hku.hk. Fax: +852 2857-1586. Tel: +852 2859-2153.

*E-mail: chanmym@hku.hk.

Notes

The authors declare no competing financial interest.

ACKNOWLEDGMENTS

V.W.W.Y. acknowledges support from The University of Hong Kong under the URC Strategic Research Theme on New Materials. This work was fully supported by a grant from the Theme-Based Research Scheme of the Research Grants Council of the Hong Kong Special Administrative Region, China (Project T23-713/11). C.Y.C. and Y.C.W. acknowledge the receipt of postgraduate studentships from The University of Hong Kong.

REFERENCES

- (1) Kaltenbrunner, M.; Sekitani, T.; Reeder, J.; Yokota, T.; Kuribara, K.; Tokuhara, T.; Drack, M.; Schwödiauer, R.; Graz, I.; Gogonea, S. B.; Bauer, S.; Someya, T. *Nature* **2013**, *499*, 458.
- (2) White, M. S.; Kaltenbrunner, M.; Glowack, E. D.; Gutnichenko, K.; Kettlgruber, G.; Graz, I.; Aazou, S.; Ulbricht, C.; Egbe, D. A. M.; Miron, M. C.; Major, Z.; Scharber, M. C.; Sekitani, T.; Someya, T.; Bauer, S.; Sariciftci, N. S. *Nat. Photonics* **2013**, *7*, 811.
- (3) Yokota, T.; Kuribara, K.; Tokuhara, T.; Zschieschang, U.; Klauk, H.; Takimiya, K.; Sadamitsu, Y.; Hamada, M.; Sekitani, T.; Someya, T. *Adv. Mater.* **2013**, *25*, 3639.
- (4) Liang, J.; Li, L.; Niu, X.; Yu, Z.; Pei, Q. *Nat. Photonics* **2013**, *7*, 817.
- (5) Sekitani, T.; Nakajima, H.; Maeda, H.; Fukushima, T.; Aida, T.; Hata, K.; Someya, T. *Nat. Mater.* **2009**, *8*, 494.
- (6) Rogers, J. A.; Someya, T.; Huang, Y. *Science* **2010**, *327*, 1603.
- (7) Liu, D.; Kelly, T. L. *Nat. Photonics* **2014**, *8*, 133.
- (8) He, Z.; Zhong, C.; Su, S.; Xu, M.; Wu, H.; Cao, Y. *Nat. Photonics* **2012**, *6*, 591.
- (9) You, J.; Dou, L.; Yoshimura, K.; Kato, T.; Ohya, K.; Moriarty, T.; Emery, K.; Chen, C.; Gao, J.; Yang, Y. *Nat. Commun.* **2013**, *4*, 1446.
- (10) Kageyama, H.; Ohishi, H.; Tanaka, M.; Ohmori, Y.; Shirota, Y. *Appl. Phys. Lett.* **2009**, *94*, 063304.
- (11) Hong, Z. R.; Lee, C. S.; Lee, S. T.; Li, W. L.; Shirota, Y. *Appl. Phys. Lett.* **2002**, *81*, 2878.
- (12) Osasa, T.; Yamamoto, S.; Matsumura, M. *Adv. Funct. Mater.* **2007**, *17*, 2937.
- (13) Alévêque, O.; Leriche, P.; Cocherel, N.; Frère, P.; Cravino, A.; Roncali, J. *Sol. Energy Mater. Sol. Cell* **2008**, *92*, 1170.
- (14) Kageyama, H.; Ohishi, H.; Tanaka, M.; Ohmori, Y.; Shirota, Y. *Adv. Funct. Mater.* **2009**, *19*, 3948.
- (15) Zheng, Y.-Q.; Potscavage, W. J., Jr.; Zhang, Q.-S.; Komino, T.; Taneda, M.; Adachi, C. *Org. Electron.* **2014**, *15*, 878.
- (16) Ma, S.; Fu, Y.; Ni, D.; Mao, J.; Xie, Z.; Tu, G. *Chem. Commun.* **2012**, *48*, 11847.
- (17) Polo, F.; Rizzo, F.; Veiga-gutierrez, M.; Cola, L. D.; Quici, S. *J. Am. Chem. Soc.* **2012**, *134*, 15402.
- (18) Li, Y. *Acc. Chem. Res.* **2012**, *45*, 723.
- (19) Son, H. J.; He, F.; Carsten, B.; Yu, L. J. *Mater. Chem.* **2011**, *21*, 18934.
- (20) Zhang, M.; Wang, H.; Tian, H.; Geng, Y.; Tang, C. W. *Adv. Mater.* **2011**, *23*, 4960.
- (21) Saragi, T. P. I.; Spehr, T.; Siebert, A.; Lieker, T. F.; Salbeck, J. *Chem. Rev.* **2007**, *107*, 1011.
- (22) Wu, C.-C.; Liu, W.-G.; Hung, W.-Y.; Liu, T.-L.; Lin, Y.-T.; Lin, H.-W.; Wong, K.-T.; Chien, Y.-Y.; Chen, R.-T.; Hung, T.-H.; Chao, T.-C.; Chen, Y.-M. *Appl. Phys. Lett.* **2005**, *87*, 052103.
- (23) Kim, J. Y.; Yasuda, T.; Yang, Y. S.; Matsumoto, N.; Adachi, C. *Chem. Commun.* **2014**, *50*, 1523.
- (24) Wong, K.-T.; Liao, Y.-L.; Lin, Y.-T.; Su, H.-C.; Wu, C.-C. *Org. Lett.* **2005**, *7*, 5131.

- (25) Liao, Y.-L.; Hung, W.-Y.; Hou, T.-H.; Lin, C.-Y.; Wong, K.-T. *Chem. Mater.* **2007**, *19*, 6350.
- (26) Dualeh, A.; Moehl, T.; Nazeeruddin, M. K.; Grätzel, M. *ACS Nano* **2013**, *7*, 2292.
- (27) Yang, L.; Xu, B.; Bi, D.; Tian, H.; Boschloo, G.; Sun, L.; Hagfeldt, A.; Johansson, E. M. J. *J. Am. Chem. Soc.* **2013**, *135*, 7378.
- (28) Heredia, D.; Natera, J.; Gervaldo, M.; Otero, L.; Fungo, F.; Lin, C.-Y.; Wong, K.-T. *Org. Lett.* **2010**, *12*, 12.
- (29) Ting, H.-C.; Tsai, C.-H.; Chen, J.-H.; Lin, L.-Y.; Chou, S.-H.; Wong, K.-T.; Huang, T.-W.; Wu, C.-C. *Org. Lett.* **2012**, *14*, 6338.
- (30) Pozzi, G.; Orlandi, S.; Cavazzini, M.; Minudri, D.; Macor, L.; Otero, L.; Fungo, F. *Org. Lett.* **2013**, *15*, 4642.
- (31) Wang, M.; Li, C.; Lv, A.; Wang, Z.; Bo, Z. *Macromolecules* **2012**, *45*, 3017.
- (32) Zhang, X.; Han, J.-B.; Li, P.-F.; Ji, X.; Zhang, Z. *Synth. Commun.* **2009**, *39*, 3804.
- (33) Zhang, H.; Cao, W.; Ma, D. *Synth. Commun.* **2007**, *37*, 25.
- (34) Lu, J.; Xia, P. F.; Lo, P. K.; Tao, Y.; Wong, M. S. *Chem. Mater.* **2006**, *18*, 6194.
- (35) Guo, L.; Li, K. F.; Wong, M. S.; Cheah, K. W. *Chem. Commun.* **2013**, *49*, 3597.
- (36) Chen, Y.-C.; Huang, G.-S.; Hsiao, C.-C.; Chen, S.-A. *J. Am. Chem. Soc.* **2006**, *128*, 8549.
- (37) Chen, G.; Sasabe, H.; Wang, Z.; Wang, X.-F.; Hong, Z.; Yang, Y.; Kido, J. *Adv. Mater.* **2012**, *24*, 2768.
- (38) Xiao, Z.; Wei, G.; Wang, S.; Zimmerman, J. D.; Renshaw, C. K.; Thompson, M. E.; Forrest, S. R. *Adv. Mater.* **2012**, *24*, 1956.
- (39) Chan, C. Y. H.; Tsung, K. K.; Choi, W. H.; So, S. K. *Org. Electron.* **2013**, *14*, 1351.
- (40) Li, N.; Lassiter, B. E.; Lunt, R. R.; Wei, G.; Forrest, S. R. *Appl. Phys. Lett.* **2009**, *94*, 023307.